A MODE-SWITCHING WIRE SYSTEM FOR THERMAL BOUNDARY LAYER MEASUREMENTS

Yuna Hattori
Max Planck Institute
for Dynamics and Self-Organization
Göttingen 37077, Germany
yuna.hattori@ds.mpg.de

Claudia E. Brunner
Max Planck Institute
for Dynamics and Self-Organization
Göttingen 37077, Germany
claudia.brunner@ds.mpg.de

Clayton P. Byers
Department of Engineering
Trinity College
Hartford, CT 06106, United States
clayton.byers@trincoll.edu

ABSTRACT

The simultaneous measurement of velocity and temperature at a single location is of great value in understanding thermal boundary layer flows. In this study, we present a novel mode-switching wire system to achieve such measurement. We alternate high- and low-current in a constant-current anemometer (CCA) in order to conduct hot- and cold-wire measurements with a single wire. Here, we discuss the design, expected response, limitations, and operation of the system with preliminary measurements conducted in both non-thermal and thermal boundary layer flows. Optimization to achieve precise semi-simultaneous velocity and temperature measurements, their calibration schemes, and to reach a higher frequency response is discussed.

MOTIVATION

Thermal boundary layer flows are ubiquitous in industrial applications as well as the lower atmosphere. Understanding the coupling between velocity and temperature fluctuations is crucial for optimizing weather forecasting and wind energy production. However, this requires precise simultaneous measurements of velocity and temperature. High-resolution velocity measurements are commonly achieved using hot-wire anemometry (Bruun, 1996). Similarly, a wire maintained at ambient temperature (in cold-wire mode) allows for high-resolution temperature measurements (Arwatz *et al.*, 2015). Traditionally, simultaneous velocity and temperature measurements are obtained by placing a hot-wire and a cold-wire in close proximity to one another. However, the spatial resolution of the resulting correlation statistics is then limited to the spacing of the two wires. Instead, by switching a single wire between hot- and cold-wire mode, velocity and temperature can be sampled at a single location (Ferreira *et al.*, 2001; Ligęza, 2020). However, the temporal resolution in this approach is determined by the switching frequency and thermal characteristics of the wire. Physically longer wires are needed to reduce end conduction effects and increase the accuracy of temperature measurements, but result in decreased spatial resolution (Mydlarski & Warhaft, 1998). The challenge is therefore to select the appropriate wire geometry as well as optimize the electrical circuitry in order to switch modes rapidly enough to capture turbulent fluctuations in both velocity and temperature. Here, we present a mode-switching system whose frequency response can be sufficiently high to study turbulent statistics in a thermal boundary layer.

THEORY OF OPERATION

The design of the system is based on Byers *et al.* (2018), using an external function generator in conjunction with a constant-current anemometry (CCA) circuit based on a Wheatstone bridge to switch the current through the wire between a high- and a low-current setting. Modifications of the circuitry can be done to allow for constant voltage anemometry (CVA) and constant temperature anemometry (CTA) to further increase the frequency response, but are not investigated in this study. By switching the current, a single wire-probe can be operated as both a hot-wire and a cold-wire. Operation of the sensor is simple and, in contrast to constant-temperature hot-wire anemometry, does not require a feedback circuit.

The CCA circuit contains a modified Wheatstone bridge in order to accurately measure any resistance change in the sensing wire under different operating modes and amplifier gain values. The voltage across the nodes in the Wheatstone bridge requires two separate amplification stages to yield an output voltage that can be recorded by an analog-to-digital converter for both hot- and cold-wire operation. The required amplification is based on the wire properties (see the next section) and energy equation of the wire. The balance resistances in the Wheatstone bridge are selected to allow for an appropriate offset to the signal such that both hot- and cold-wire signals are resolvable.

Circuitry Design and Characteristics

A regular Wheatstone bridge is limited in use for both hot- and cold-wire modes due to competing balancing needs; the hot-wire mode overheats the wire, so electrical balance in a Wheatstone bridge in this mode would result in a significant

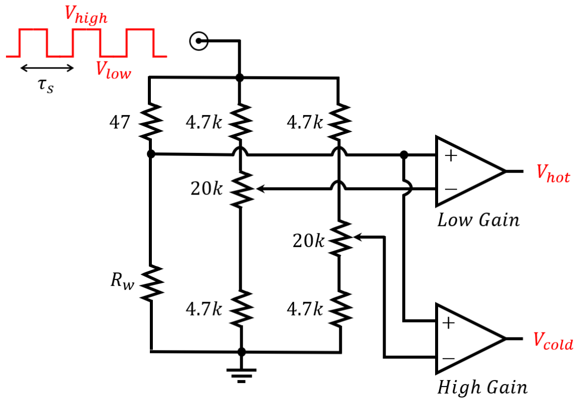

Figure 1: Simplified schematic for the switching system. Red text signifies voltages, and all resistor values are in Ohms.

imbalance when switched to cold-wire mode. Additionally, the high gain needed for the cold-wire mode would result in this imbalance yielding unusable signals by saturating the amplifier output. Therefore, a modification is made to include two separate balancing legs for the switching circuitry, shown in Fig. 1. This simplified schematic shows two separate balancing potentiometers to allow both the low gain amplifier (for the hot wire signal) and the high gain amplifier (for the cold wire signal) to be balanced when in their appropriate operating regime. These two balancing legs form a high resistance pathway such that the current through them is both small and nearly constant. An external square wave voltage is sent to the circuit to drive the operating mode of the wire, whose ambient resistance is $R_w = 45.6\,\Omega$ at $T_0 = 20°C$. With the signal switching between $V_{high} = 200\,mV$ and $V_{low} = 5\,mV$, the wire is subjected to approximately $2.066\,mA$ and $0.052\,mA$ of current in the hot- and cold-wire modes, respectively. The amplifiers are set to a gain of 390 and 10332 for the low and high gain, respectively. Two capacitors are placed before the power supply for the amplifiers, reducing any potential electromagnetic noises. The switching time for the operating mode is set to $\tau_s = 2\,ms$, or equivalently $f_s = 500\,Hz$. This time scale is sufficiently larger than the time scale of the wire, as shown in the next section, allowing the wire to come into thermal equilibrium with the flow after a step change in current.

Wire Specification

The energy balance in the wire is dominated by convective heat transfer and Joule heating. Ignoring any end conduction effects (to be justified later), the energy equation for the wire is,

$$m_w c_w \frac{dT_w}{dt} = I^2 R_w - h_w A_w (T_w - T_\infty), \tag{1}$$

where I is the current passing through the wire, R is the wire resistance, and the subscript w refers to properties associated with the wire. The resistance of the wire changes with temperature, where $R = R_0\,(1 + \alpha(T - T_0))$ for initial resistance R_0 at temperature T_0, and thermal coefficient of resistance $\alpha = 0.0036\,K^{-1}$. Furthermore, the convective heat transfer coefficient can be determined from the Nusselt number (Nu) using an empirical relation for a cylinder in cross flow from Chang & Finlayson (1987) assuming room temperature air as the working fluid,

$$h_w = \frac{kNu}{d} \quad \text{and} \quad Nu = 0.39Re_d^{0.05} + 0.45Re_d^{0.51}, \tag{2}$$

where k is the thermal conductivity of the fluid, d is the diameter of the wire, and $Re_d = U_\infty d/\nu$ is the Reynolds number based on the wire diameter, velocity of the free stream U_∞, and kinematic viscosity of the fluid ν.

To determine the frequency response of the wire, the time constant for the system can be approximated through an order of magnitude analysis of equation 1:

$$\tau \propto \frac{m_w c_w}{h_w A_w} = \frac{d^2 \rho_w c_w}{4kNu}, \tag{3}$$

where ρ_w is the density of the wire material and k is the thermal conductivity of the fluid. Using a Dantec cold wire made of platinum (55P31) with length $l = 400\,\mu m$, diameter $d = 1\mu m$, density $\rho_w = 21450\,kg/m^3$, and $c_w = 133\,J/(kgK)$, this thermal time constant ranges from $\tau = 5.314 \times 10^{-5}\,s$ at $U_\infty = 2\,m/s$ to $3.484 \times 10^{-5}\,s$ at $U_\infty = 12\,m/s$ seconds, giving a $-3\,dB$ cutoff frequency of 3 kHz to 4.5 kHz depending on the flow speed, sufficiently fast to equilibrate with the flow when switching operating modes at 500 Hz. Additionally, the end conduction effects can be assessed using the Γ criterion developed by Hultmark *et al.* (2011). For this wire geometry $\Gamma \approx 13.6$, which is at the lower limit to avoid velocity signal attenuation.

Under the assumption of steady state operation in the low current mode, equation 1 shows an increase of the wire temperature due to Joule heating of $\Delta T_w \leq 0.01°C$ at 0.5 m/s airflow, confirming cold-wire operation. Higher velocities will yield lower temperature differences.

Boundary Layer Facility

Thermal boundary layer measurements are conducted in the Prandtl Wind Tunnel (PWT) at the Max Planck Institute for Dynamics and Self-Organization in Göttingen, Germany. A schematic of the experimental setup is shown in Fig. 2. The test section has a length of 8 m, a width of 1.5 m, and a height of 1 m. The air flow induced by the fan passes through an active turbulence grid, develops a boundary layer over an unheated surface (6 m) and finally passes over a heated surface (2 m). This heated surface was originally developed by Nunnari (2021). It has a plate thickness of $L_c = 2.54$ cm and a surface heat conductivity of $k_s = 237$ W/(m K), resulting in a Biot number of $Bi = hL_c/k_s < 1.33 \times 10^{-3}$ (here h is the convection coefficient of the boundary layer, estimated following the approach of Zhukauskas & Ambrazyavichyus (1961) to account for an unheated entrance region), indicating that the plate will maintain a constant temperature throughout the surface. A PID controller was used to set and maintain the surface temperature, and the high thermal mass of the surface resulted in a steady and consistent T_w value.

The active turbulence grid can be used to generate specific turbulence statistics in the freestream (Bodenschatz *et al.*, 2014). For the results shown within, the active grid was kept fully open, functioning as a passive grid. The freestream turbulence level was measured as $u'_{rms}/U_\infty = 0.15$, a consequence of the large mesh size of the grid. While the high turbulence level will mean that canonical zero-pressure-gradient boundary layer theory may not hold, the function of the switching wire system is still applicable.

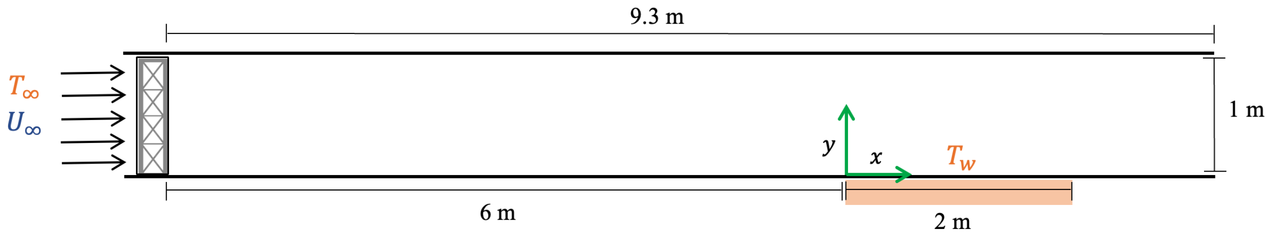

Figure 2: Schematic of the experimental setup inside the Prandtl Wind Tunnel (PWT). The flow with a freestream temperature T_∞ and a freestream velocity U_∞ induced by the fan passes through an active turbulence grid and then develops a boundary-layer before reaching the heated region with a constant surface temperature T_w.

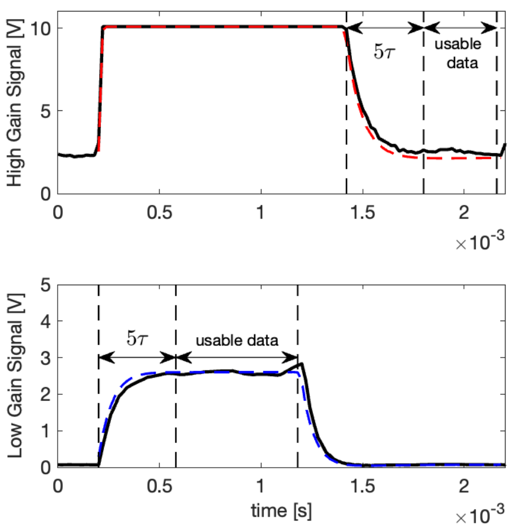

Figure 3: Extraction of relevant data from the two signals. Upper plot shows high gain signal used for the temperature, lower plot shows the low gain signal used for the velocity, both in solid black lines. Usable data is indicated as the range following five time constants as extracted from the wire response. Dashed color curves are the phase averaged waveforms. Horizontal dashed-dot line indicates mean of all usable data in the time series.

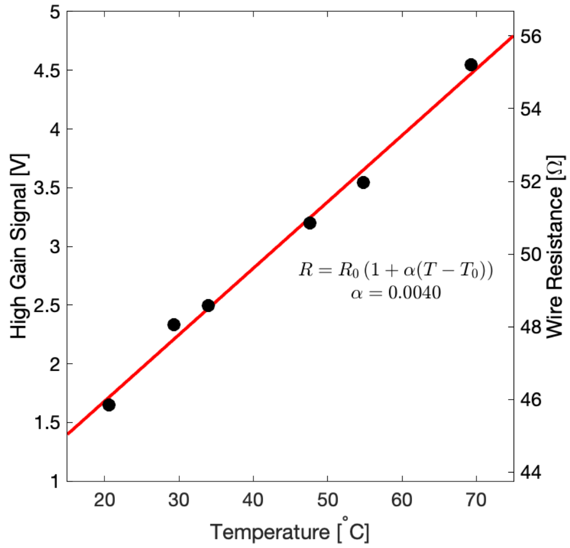

Figure 4: Calculation of coefficient of resistance for the wire.

RESULTS

Extraction of the velocity and temperature signals is performed through a conditional averaging of the high voltages in the low gain signal and the low voltages of the high gain signal, respectively. An example can be seen in Fig. 3, where the cold wire (high gain) signal is shown on top and the hot wire (low gain) signal is on bottom. Phase averaging is performed to extract the average waveform over each time series, shown as the dashed color line in each plot. Using the exponential portion during switching from low to high current for the hot-wire, and high to low current for the cold-wire, the time constant for decay is extracted, with $\tau_{cold} = 7.73 \times 10^{-5}$ and $\tau_{hot} = 8.52 \times 10^{-5}$ seconds when operated at $U_\infty = 4\,m/s$. These are slightly longer than the estimated time constants from equation 3, likely due to end-conduction effects, but the same order of magnitude. Using the values of τ for each mode of operation, a delay of 5τ is imposed before any data is extracted. The usable data range ends when the next mode switch is detected. These ranges are highlighted in Fig. 3. Note that there is less usable time for the cold wire (high gain) signal due to the saturated amplifier output delaying the time at which 5τ can be accounted for. This methodology is employed on each time series in calibration and boundary layer measurements to obtain the flow statistics.

Calibration

Verification of the thermal properties of the wire was performed by placing it coincident with a thermistor using a heated stream at various temperatures. The switching system was run for a period of 30 seconds at a given temperature and the usable data from the high gain signal was extracted following the methodology detailed previously. The thermistor was calibrated with a thermal bath to ensure accuracy of temperature readings up to 100 $°C$. The results are shown in Fig. 4, where the voltage was converted to a resistance by using the values of the balance resistors, the applied voltage, and set amplifier gains. This calibration resulted in a temperature coefficient of $\alpha = 0.004 \pm 0.0003$ $1/°C$, which is higher than the stated factory value of the wire. However, there is uncertainty in this calculation as the applied voltage to the bridge,$V_{low} = 5\,mV$, could be slightly altered due to impedance mismatching between the function generator and the circuit.

The hot wire calibration took place using both a Dantec Dynamics "calibration box" and with in-situ measurements coincident with a Pitot tube measurements in the wind tun-

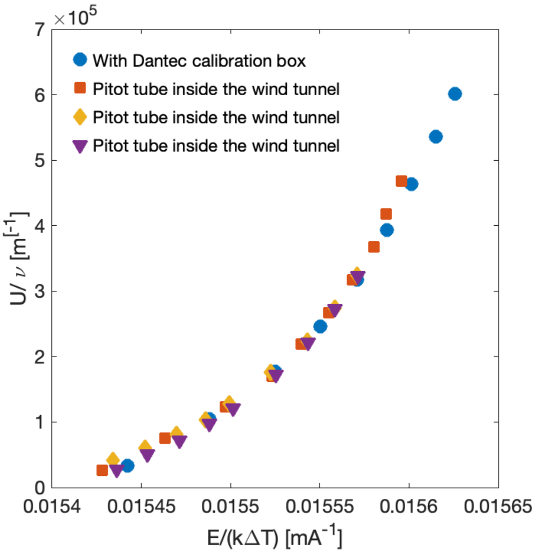

Figure 5: Calibration of hot wire mode, each conducted on different days.

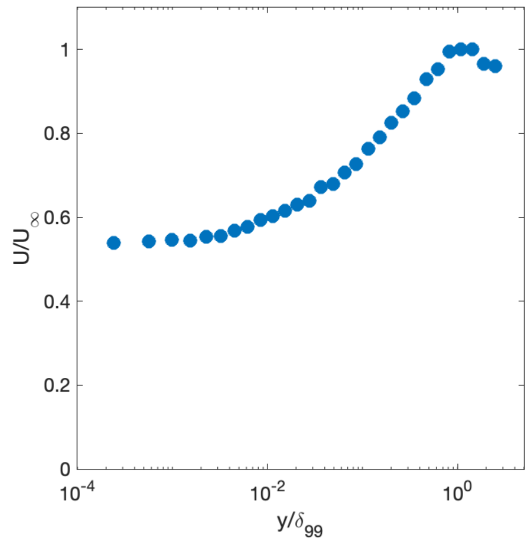

Figure 6: Velocity profile normalized in outer units, obtained in no plate heating case. Boundary layer thickness found to be $\delta_{99} = 99.6$ mm.

nel. The hot wire is calibrated in the tunnel before and after profile acquisition. All data is plotted in Fig. 5 using the normalization scheme of Hultmark & Smits (2010). Before applying this normalization, we made a linear correction to the calibration curve to account for a drift in the signal, resulting in a constant offset voltage between different data collection runs. Ambient temperature was measured during calibration runs and used to calculate the thermal conductivity and kinematic viscosity from NIST Reference Fluid Thermodynamic and Transport Properties Database (Lemmon *et al.*, 2018).

Velocity and Temperature Profiles

We conducted our measurements for two cases: (I) without plate heating to use our switching system and data extraction scheme with the low-gain signal, and (II) with floor heating to see the thermal boundary layer through the data extraction scheme on the high-gain signal. The freestream velocity for these tests was $U_\infty = 4.15$ m/s, and the downstream measurement location was 7.84 m from the leading edge with 1.84 m of heated wall. Case I was done with $T_\infty = 20.07$ °C, and Case II with $T_w = 40.05$ °C and $T_\infty = 21.26$ °C. The Reynolds number based on momentum thickness is calculated to be $Re_{\delta_2} \approx 4300$ from integration and $u_\tau \approx 0.229$ m/s from the $1/7^{th}$ power law. These values are only approximate, as the wall-normal location was not accurately known at the time of data collection, introducing uncertainty in the integration for δ_2 but remaining within 10% of an estimate using the $1/7^{th}$ power law. These results provide an estimated large scale outer frequency of $f_o = U_\infty/2\pi\delta = 6.5$ Hz, and an estimated maximum frequency content in the flow of $f_{max} \approx 1100$ Hz following Hutchins *et al.* (2009).

Figure 6 shows the mean streamwise velocity profile normalized in outer coordinates for Case I: unheated boundary layer. Here y is the distance from the wall, and δ_{99} is taken as $U(\delta_{99}) = 0.99U_\infty$. The measurements demonstrate that the lowest wall-normal placement of the wire is still outside of the viscous sub-layer, contributing to the error in the estimate of δ_2. There is some residual offset visible in the signal in the freestream. The potential fixes for these will be addressed in the subsequent section.

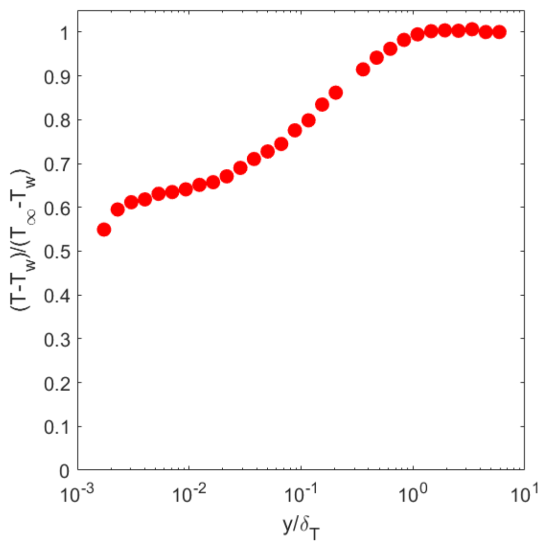

Figure 7: Temperature profile normalized in outer units. Thermal layer thickness found to be $\delta_T = 53.1$ mm.

Figure 7 shows the mean non-dimensional temperature profile $(T(y) - T_\infty)/(T_w - T_\infty)$ above the heated plate in Case II. Here T_∞ is the freestream temperature, T_w is the temperature at the wall, and δ_T is the location that the temperature deficit reaches 99% of the freestream. The measurements demonstrate that the temperature distribution follows the expected thermal boundary layer profile when scaled with outer units, validating the signal extraction method. However, the velocity profile from this data set is not presented due to issues with the circuit and data processing.

CONCLUSIONS AND ONGOING WORK

While the switching methodology and data extraction for the two separate signals works and produces the mean profiles for both U and T, there are several improvements to be made to both the circuitry and the post-processing that will allow for all statistics related to the streamwise velocity, temperature, their co-variances, and associated spectral content.

Ongoing work in the circuit design is aimed at improving performance and repeatability. The circuit used in this study has suffered from both drift in the output signal and interference from 50 Hz noise present in the facility power. A new design changes the switching operation to an externally driven function generator that enables or disables a transistor switch, bringing in a constant current source and removing the function generator from the signal path affecting the hot- and cold-wire. The present methodology uses a function generator to drive the circuit and hot wire, and is subjected to impedance mismatching and instability of the voltage. These have resulted in drifting signals when performing repeated measurements under the same facility conditions. With two independent constant current sources, one switched in and out from an external source, a more stable operation will be able to take place. Additionally, the voltage drop over the wire is currently backed out using the Wheatstone bridge equations under the assumption of ideal component values. The new system will provide a reference voltage that is compared to the voltage over the wire itself, allowing a direct calculation of the wire resistance and therefore the freestream temperature and calibration scheme for the velocity.

Using the new circuit, the thermal calibration will also be improved through a modified experimental setup to better stabilize the incoming temperature stream. Instability in the temperature source, in addition to the previously mentioned design issues with the circuit, resulted in increased uncertainty in the value of α, affecting the velocity calibration with the thermal boundary layer.

These improvements will then allow the calculation of $\overline{u'T'}$ by correlating the temperature with velocity at a delay of approximately 5τ, or ≈ 0.42 ms in the experimental conditions described here. The switching frequency effectively limits the spectral content that can be obtained and is in turn driven by the thermal response characteristics of the wire. As such, the switching frequency of this system is limited to around 1000 Hz under these experimental conditions. This would result in a spectral content limited to 500 Hz, which could be useful for atmospheric measurements or lower speed wind tunnel tests.

ACKNOWLEDGEMENT

This work was funded by the Deutsche Forschungsgemeinschaft (DFG, German Research Foundation) 555568385. We would like to thank Ms. Laura Diaz Rodriguez and Dr. Holger Nobach from the electonics section, Mr. André Heil and his machine shop section, and Mr. Andreas Renner at Max Planck Institute for Dynamics and Self-Organization.

REFERENCES

Arwatz, Gilad, Fan, Yuyang, Bahri, Carla & Hultmark, Marcus 2015 Development and characterization of a nano-scale temperature sensor (t-nstap) for turbulent temperature measurements. *Measurement Science and Technology* **26** (3), 035103.

Bodenschatz, Eberhard, Bewley, Gregory P, Nobach, Holger, Sinhuber, Michael & Xu, Haitao 2014 Variable density turbulence tunnel facility. *Review of Scientific Instruments* **85** (9).

Bruun, Hans H 1996 Hot-wire anemometry: principles and signal analysis. *Measurement Science and Technology* **7** (10), 024.

Byers, Clayton P, Fu, Matthew K, Fan, Yuyang & Hultmark, Marcus 2018 Development of instrumentation for measurements of two components of velocity with a single sensing element. *Measurement Science and Technology* **29** (2), 025304.

Chang, Michael Wei & Finlayson, Bruce A 1987 Heat transfer in flow past cylinders at re< 150—part i. calculations for constant fluid properties. *Numerical Heat Transfer, Part A: Applications* **12** (2), 179–195.

Ferreira, Romulo Pires Coelho, Freire, Raimundo Carlos Silvério, Deep, CS, de Rocha Neto, Jose Sérgio & Oliveira, Amauri 2001 Hot-wire anemometer with temperature compensation using only one sensor. *IEEE Transactions on Instrumentation and Measurement* **50** (4), 954–958.

Hultmark, Marcus, Ashok, Anand & Smits, Alexander J 2011 A new criterion for end-conduction effects in hot-wire anemometry. *Measurement Science and Technology* **22** (5), 055401.

Hultmark, Marcus & Smits, Alexander J 2010 Temperature corrections for constant temperature and constant current hot-wire anemometers. *Measurement Science and Technology* **21** (10), 105404.

Hutchins, Nicholas, Nickels, Timothy B, Marusic, Ivan & Chong, MS 2009 Hot-wire spatial resolution issues in wall-bounded turbulence. *Journal of Fluid Mechanics* **635**, 103–136.

Lemmon, E. W., Bell, I. H., Huber, M. L. & McLinden, M. O. 2018 NIST Standard Reference Database 23: Reference Fluid Thermodynamic and Transport Properties-REFPROP, Version 10.0, National Institute of Standards and Technology.

Ligęza, Paweł 2020 Modification of hot-wire anemometers frequency bandwidth measurement method. *Sensors* **20** (6), 1595.

Mydlarski, Laurent & Warhaft, Zellman 1998 Passive scalar statistics in high-péclet-number grid turbulence. *Journal of Fluid Mechanics* **358**, 135–175.

Nunnari, Giuseppe Gabriele 2021 Experimental investigation of a sheared thermally unstable boundary layer. PhD thesis, Dissertation, Göttingen, Georg-August Universität, 2021.

Zhukauskas, AA & Ambrazyavichyus, AB 1961 Heat transfer of a plate in a liquid flow. *International Journal of heat and mass transfer* **3** (4), 305–309.